ACS APPLIED MATERIALS & INTERFACES

Research Article

www.acsami.org

Fluorescent Graphene Oxide via Polymer Grafting: An Efficient Nanocarrier for Both Hydrophilic and Hydrophobic Drugs

Aniruddha Kundu, Sudipta Nandi, Pradip Das,‡ and Arun K. Nandi*

Polymer Science Unit, Indian Association for the Cultivation of Science, Jadavpur, Kolkata 700 032, India

Supporting Information

ABSTRACT: Functionalized graphene-based drug delivery vehicles have conquered a significant position because functionalization improves its biocompatibility and stability in cell medium, leaving sufficient graphitic basal plane for drug loading through $\pi-\pi$ stacking. In this study, poly(*N*-isopropylacrylamide) (PNIPAM) is covalently grafted from the surface of graphene oxide (GO) via a facile, eco-friendly and an easy procedure of free radical polymerization (FRP) using ammonium persulfate initiator. Various spectroscopic and microscopic studies confirm the successful grafting of PNIPAM from GO surface. PNIPAM-grafted GO (GPNM) exhibits enhanced thermal stability, improved dispersibility both in aqueous and cell medium, and better biocompatibility and cell viability compared to GO. Interestingly, GPNM displays an exciting fluorescence property in aqueous medium, which is a hike of intensity at 36 °C due to the lower critical solution temperature (LCST) of PNIPAM chains (32 °C). Moreover both hydrophilic (doxorubicin (DOX)) and hydrophobic (indomethacin (IMC)) drugs loaded on the surface of GPNM hybrid exhibits its efficacy as an efficient carrier for both types of drugs. Cellular uptakes of free DOX and DOX-loaded GPNM (GPNM-DOX) are evidenced both from optical and fluorescence imaging of live cells, and the efficiency of drug is significantly improved in the loaded system. The release of DOX from GPNM-DOX was achieved at pH 4, relevant to the environment of cancer cells. The pH-triggered release of hydrophobic drug was also studied using UV−vis spectroscopy via alginate encapsulation, showing a great enhancement at pH = 7.4. The IMC is also found to be released by human serum albumin using dialysis technique. The GPNM nanomaterial shows the property of simultaneous loading of DOX and IMC as well as pH-triggered simultaneous release of both of the drugs.

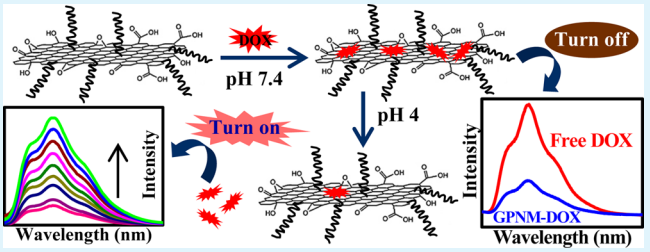

KEYWORDS: *free radical polymerization, fluorescence, doxorubicin, cellular uptake, drug delivery*

INTRODUCTION

Recently, graphene oxide (GO) has sparked an enormous interest in the scientific and technological community due to its intriguing electronic, mechanical, thermal, and optical properties.[1−7] It can easily be made from graphite, which is an abundant and cheap material, and it appears to be the precursor of its counterpart graphene. GO has the natural tendency to be highly dispersible both in water and in polar organic solvent due to the presence of oxygen-containing group at the basal plane as well as at the edges of graphene.[8−10] Poor dispersibility of graphene in common solvents and its intrinsically zero band gap prohibit any spectral transition limiting its applications in the fields like fabrication of optoelectronic devices, chemo/biosensing, etc. But the existence of substantial band gap in GO due to the presence of sp^3-hybridized carbon atoms[11−13] makes it a smart nanomaterial with the possibility of application in different fields. Its distinct characteristics, such as large surface area and facile surface modification,[14−16] provide the opportunity of tailoring the optoelectronic properties of GO.[17] All the aforementioned advantages of GO make it extremely attractive in nanocomposites[6,18] and catalysis,[19] and they have also opened up exciting ways of exploiting new applications in biotechnology, such as drug delivery, cell imaging,[20−22] chemo/biosensing,[23] etc.

The research field of GO that has gained recent popularity is the fluorescence property, arising from the heterogeneous atomic and electronic structures of GO. Dai and his coworkers[20,21] have reported the intrinsic fluorescence property of nanographene oxide (NGO) for the first time. Then several research groups have reported the fluorescence property of GO and functionalized GO, which was presumably allocated to the radiative recombination of electron−hole pairs among the confined cluster originating from the small and isolated sp^2 carbon domains embedded in the sp^3 matrix.[17,24−27] Recently, the pH-dependent fluorescence property of GO has also been explored,[28−30] which opens a new way to develop different efficient chemical and biochemical sensors.[31,32] In the previous articles, we exploited the pH-dependent fluorescence property of GO to make highly fluorescent GO polymer hybrids, which have been used as efficient fluorescent materials to detect nitroaromatics and Au^{3+} ion.[33,34] We have also reported the

Received: October 15, 2014
Accepted: January 23, 2015
Published: January 23, 2015

DOI: 10.1021/am507110r
ACS Appl. Mater. Interfaces 2015, 7, 3512−3523

pH-dependent fluorescence property of functionalized graphene, namely, sulfonated graphene (SG), and it has been used as a donor to detect vitamin B_2 in the fluorescence resonance energy transfer-based system.[35] Fluorescence property of GO-polymer hybrid/functionalized GO at low pH restricted us to further apply this nontoxic, cheap fluorescent material for biological applications. Recently, the applicability of functionalized GO in biomedical field increases utilizing its high surface area that enables to load various kinds of drug via noncovalent interaction. Though GO may exhibit some biocompatibility due to its oxygen-containing groups, polymer-functionalized NGO has been successfully used as a nanocarrier to load anticancer drugs where polymer attachment improves the biocompatibility as well as stability of graphene sheets in biological medium.[20,21] Considering these well-documented facts, here we covalently functionalized GO using a commonly used biocompatible polymer to render the GO stable in aqueous solution, biocompatible, and highly fluorescent at neutral pH.

In recent days different radical polymerization techniques are employed for the grafting of several types of polymer chains from or onto GO sheets via "grafting from", "grafting to" or in situ polycondensation approaches,[36−44] and attention has been paid to the functionalization of graphene or GO mainly for improving their dispersibility. Although controlled radical polymerization (CRP) techniques such as atom transfer radical polymerization (ATRP),[36,39] reversible addition−fragmentation chain transfer (RAFT),[45] and single electron transfer-living radical polymerization (SET-LRP)[46] are used to graft definite polymer chains on graphene or GO surfaces, but these procedures are quite complicated since extra steps are necessary to introduce initiating groups on graphene or GO sheets before the process of grafting. Recently Pan et al. have synthesized water-soluble poly(*N*-isopropylacrylamide) grafted graphene sheets via click chemistry for hydrophobic drug delivery,[47] but the synthetic procedure is much too lengthy and hazardous. For this reason we used the simple in situ free radical polymerization (FRP) technique to graft poly(*N*-isopropylacrylamide) (PNIPAM) from GO surface using the previously reported methods.[44,48] We selected *N*-isopropylacrylamide (NIPAM) as monomer to prepare GO-PNIPAM (GPNM) hybrids to enhance the aqueous dispersibility of GO since NIPAM is a well-known hydrophilic monomer. Also PNIPAM, a biocompatible and stimuli-responsive polymer, has potential biomedical applications, such as controlled drug delivery, artificial muscles, cell adhesion mediators, and precipitation of proteins.[49,50] Recently, functionalized GO has found fascinating applications in drug delivery.[51−55]

In this article we report the fluorescence property of GPNM hybrids in aqueous medium and investigate the origin of the enhanced fluorescence property. We also studied the in vitro cytotoxic effect of as-synthesized GPNM hybrid by measuring the relative cell viability using conventional methyl thiazolyl tetrazolium (MTT)-based assay. Owing to the presence of conjugated structure and oxygenous moiety in GO basal plane, GPNM can adsorb and attach both hydrophilic and hydrophobic aromatic drugs via $\pi-\pi$ stacking, hydrophobic, and hydrogen bonding interactions. So, we investigated the loading and release behavior of a hydrophilic anticancer drug doxorubicin (DOX) by using the fluorescence property as well as a water-insoluble, nonsteroidal anti-inflammatory drug indomethacin (IMC) via UV−vis spectroscopy. The cellular uptake of free DOX and DOX-loaded GPNM (GPNM-DOX) are studied to understand the efficiency of GPNM as a nanocarrier. On the other hand, pH-triggered release of IMC is carried out utilizing the encapsulating ability of sodium alginate (SA), which is a significant ingredient to construct oral drug delivery vehicle.[56] The individual release of IMC to human serum albumin (HSA) is also studied using dialysis technique. To the best of our knowledge, the GO-grafted smart polymers or functionalized GO can act as nanocarrier for one kind of drug, either hydrophilic or hydrophobic, as reported in recent literature.[47,52,55] Here the present GPNM nanocarrier was successfully employed to load both types of drugs (hydrophilic and hydrophobic) having different clinical functions. We also studied the possibility of simultaneous delivery of the drugs using our synthesized GPNM nanocarrier.

EXPERIMENTAL SECTION

Materials. Graphite powder, *N*-isopropylacrylamide, and HSA were purchased from Sigma-Aldrich (USA). Potassium permanganate, 35% hydrochloric acid (G.R. grade), sulfuric acid, phosphoric acid, 30% hydrogen peroxide, sodium alginate (SA), calcium chloride, Tris·HCl, and ammonium persulfate (APS) were purchased from Merck (Mumbai) and were used as received.

Synthesis of GO and GO-*g*-PNIPAM (GPNM) Hybrids. At first graphite oxide was prepared from graphite powder according to the improved Hummers method[57] and sonicated in water to prepare well-exfoliated GO sheets. PNIPAM was grafted onto GO via the in situ free radical polymerization.[44] Typically 10 mg of GO and 20 mL of high-performance liquid chromatography (HPLC)-grade water were taken in a round-bottom flask, sonicated for 1 h in an ultrasonic bath (60 W, frequency 28 kHz, model AVIOC, Eyela) to obtain a well-dispersed solution. Then the required amounts of NIPAM and HPLC-grade water were added to the flask and stirred for 30 min, followed by the addition of 50 mg of APS (initiator). The resulting solution was purged with nitrogen for 30 min and was then immersed in an oil bath thermostated at 65 °C. After 48 h the reaction mixture was cooled to room temperature and exposed to air to terminate the reaction. The solution was then centrifuged at the speed of 12 000 rpm using a Beckman Coulter (Allegra Model 64R) centrifuge and repeatedly washed with cold water to remove the noncovalently attached free polymers to GO until the supernatant becomes transparent, tested at hot condition (~35 °C). The resulting products were then freeze-dried and stored in vacuum for further use. The recipes of the preparation of different GPNM hybrids are presented in Supporting Information, Table S1, and the schematic outline is delineated in Scheme 1. The GPNM 1:50 (w/w) hybrid is commonly designated as GPNM hybrid, which is used for different drug-loading and drug-delivery purposes.

Scheme 1. Schematic Representation of the Synthesis of GO-g-PNIPAM Using in Situ FRP Technique

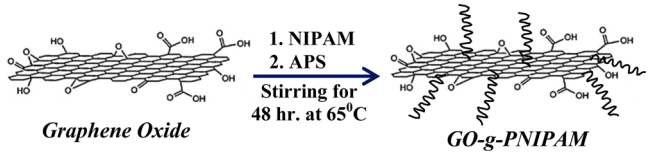

Instrumentation. *Microscopy.* The GO and GPNM dispersions were characterized by transmission electron microscopy (TEM JEOL, 2010EX) fitted with a CCD camera at an acceleration voltage of 200 kV. The samples for TEM measurements were prepared by casting a small drop of dilute GO and GPNM solution on a carbon-coated copper grid, allowed to dry in air, and finally dried in vacuum at 30 °C. Atomic force microscopy (AFM) was conducted in the noncontact mode at a resonance frequency of ~250 kHz of the tip. A drop of dilute sample solution (GO and GPNM1:50) was casted on a clean mica surface, and the morphology of the vacuum-dried sample was studied using an AFM instrument (Veeco, model AP 0100).

DOI: 10.1021/am507110r
ACS Appl. Mater. Interfaces 2015, 7, 3512−3523

Spectroscopy. The GO and GPNM hybrids were dispersed in desired amount of HPLC-grade water and sonicated in an ultrasonic bath to make a constant composition (0.01% w/v) for spectroscopic studies. The UV−vis absorption spectra of aqueous solutions of the samples were recorded with a UV−vis spectrophotometer (Hewlett-Packard, model 8453) using a cuvette of 1 cm path length. For temperature-dependent absorbance measurement the pure PNIPAM and GO-*g*-PNIPAM (GPNM 1:50) hybrid solution was equilibrated for 10 min at each temperature.

Fluorescence (FL) study was performed in a sealed cuvette, and the emission was recorded in a Horiba Jobin Yvon Fluoromax 3 instrument. GO and GPNM hybrid solutions were taken in a quartz cell of 1 cm path length, excited at 320 nm wavelength, and the emission scans were recorded from 350 to 610 nm using a slit width of 5 nm for both the excitation and emission with an increment of 1 nm wavelength having an integration time of 0.1 s. For loading and release study of DOX the sample solutions were excited at 490 nm wavelength, and the emission scans were recorded from 510 to 800 nm with the same slit width as above.

The ^{1}H NMR spectra of different GPNM hybrids (0.1 mg/mL) were performed using Bruker spectrometer operating at 500 MHz in D_2O.

FTIR spectra of GO and GPNM hybrids were obtained using KBr pellets of the solid samples in Perkin Elmer FTIR instrument (spectrum100).

Raman spectra of GO and different GPNM hybrids were recorded using a LabSpec Raman spectroscope (JY T6400). The sample solutions were taken in a quartz cell of 1 cm path length and were excited using 514 nm argon laser with a scanning duration of 50 s.

The X-ray photoelectron spectroscopic (XPS) study of the GO and GPNM 1:50 hybrid film was performed using a focused monochromatized Mg Kα X-ray source (1253.6 eV) in the XPS instrument (Omicron NanoTechnology 0571).

Thermogravimetric Analysis. The thermal stability of GO and GPNM1:50 were measured using a Perkin Elmer TGA instrument (Pyris Diamond TG/DTA) under nitrogen atmosphere at a heating rate of 10 °C min^{-1}.

Cellular Uptake Study. The uptake of free DOX and DOX-loaded GPNM hybrid (GPNM-DOX) by human glioblastoma cells U87MG was evaluated by fluorescence microscopy. The U87MG cells were seeded in 24-well tissue culture plates in the presence of 500 μL of Dulbecco's modified Eagle medium (DMEM) containing 10% fetal bovine serum (FBS) and 1% penicillin/streptomycin at 37 °C and 5% CO_2. After overnight growth, the cells were incubated for 6 h with free DOX and GPNM-DOX at final concentration of drug (8.5 μg/mL). After washing the cells with PBS buffer solution, fresh DMEM medium was added, and live cells were imaged under fluorescence microscope in green light excitation.

Loading and Release of DOX. Loading of DOX onto GPNM hybrid was carried out by simply mixing various amounts of DOX (0.025 to 0.1 mg/mL) with GPNM solution of different concentrations (0.1 to 0.3 mg/mL) at pH 7.4 and was kept overnight with stirring. Unbound excess DOX was removed by centrifugation at 15 000 rpm for 10 min. The supernatant was discarded, and the precipitate (GPNM-DOX) was washed three times with HPLC-grade water by centrifugation. Then the resulting complexes were resuspended and were stored at 4 °C for future use. The loading of DOX was investigated by fluorescence and UV−vis spectroscopy. For release of DOX, the GPNM-DOX was incubated in buffer solutions at pH 4 for different periods of time. The release of DOX from GPNM-DOX was monitored by fluorescence spectroscopy using the supernatants from GPNM-DOX after centrifugation at different time points at 30 °C.

In Vitro Cytotoxicity Assays and Biocompatibility Evaluation. The relative cell viability of GO and GPNM in U87MG cells and mouse embryonic fibroblasts cells (3T3-L1) was evaluated by conventional 3-(4,5-dimethylthiazol-2-yl)-2,5-diphenyltetrazolium bromide (MTT) assays, assuming 100% cell viability for control cells, that is, without any materials. The in vitro cytotoxicity of DOX and GPNM-DOX on U87MG cells were also studied by MTT assay. At first, GO and GPNM solutions were dialyzed against HPLC-grade water to remove any soluble impurity or free homopolymer before cytotoxicity measurement. Then, the U87MG and 3T3-L1 cells were seeded in 24-well plates at high density in 500 μL of DMEM containing 10% FBS and 1% penicillin/streptomycin at 37 °C and 5% CO_2. After overnight of cell attachment, the cells were incubated with different GO and GPNM concentrations (2−100 μg/mL) for 24 h. For free DOX and GPNM-DOX the concentration of DOX was varied (1−22 μg/mL) for the in vitro cell viability study. The unbound materials were removed by washing with PBS buffer solution. Then 500 μL of DMEM medium was added to each well, and 50 μL of aqueous solution of MTT (5 mg/mL) was added and allowed to stand for 4 h. The violet formazan was dissolved in 500 μL of sodium dodecyl sulfate solution in water/dimethylformamide mixture. Absorbance of formazan solution was carried out at 570 nm using a BioTek SynergyMx microplate reader.

The effect of GO, GPNM, DOX, and GPNM-DOX on the cell morphology was observed by optical microscope. Briefly, the cells were seeded in 24-well plate in 500 μL of DMEM medium supplemented with 10% FBS and 1% penicillin/streptomycin at 37 °C and 5% CO_2. After overnight growth, the cells were incubated with GO and GPNM of final concentration of 17 μg/mL for 24 h. In the case of DOX and GPNM-DOX the final concentration of DOX was 8.5 μg/mL. Then cells were washed with PBS buffer solution to remove the uninternalized materials. Then fresh 500 μL of above DMEM medium was added. The cell morphology was observed by using Olympus IX81 optical microscopy.

Loading and Release of Indomethacin. Indomethacin (IMC) capsule was dissolved in 2 mL of alcohol, shaken vigorously, and then centrifuged at 4000 rpm for 10 min. The yellowish colored supernatant was collected. The residue was washed with 3 mL of alcohol using centrifuge, and a total of 5 mL of solution was collected and stored in refrigerator as stock solution. For loading purpose different amount of alcoholic indomethacin solution was added to same quantity of aqueous GPNM solution keeping the GPNM concentration as 0.2 mg/mL, and the indomethacin concentrations were varied from 0.01 to 0.1 mg/mL. The loading of indomethacin was investigated by UV−vis spectroscopy. For release of the hydrophobic drug two techniques were adopted. In the first case, IMC-loaded GPNM (GPNM-IMC) solution was used to prepare sodium alginate (SA)-encapsulated GPNM-IMC beads. For that purpose 1 mL of GPNM-IMC (0.1 mg/mL) solution was added with 1 mL of SA (20 mg/mL) solution under constant stirring to get a homogeneous solution. The resultant solution was then added dropwise into $CaCl_2$ solution with gentle stirring to prevent bead agglomeration. The beads were then washed with doubly distilled water several times. After that, HCl solution was added dropwise to adjust the pH of the release media to 2, and the release of IMC was monitored using UV−vis spectra of the solution in different time interval. After 3 h tris(hydroxymethyl)aminoethane solution was added dropwise to the above solution, the pH of the release media was maintained at 7.4, and the drug release at this pH was monitored using the above-mentioned procedure. For another study GPNM-IMC solution was dialyzed against HSA solution of concentration 0.5 mg/mL, and the release of IMC from the GPNM surface was monitored by taking UV−vis spectra of the dialysate at different time interval.

Simultaneous Loading and Release of Drugs. The simultaneous loading of DOX and IMC was achieved from previously stored GPNM-DOX solution by adding alcoholic solution of IMC (concentration of drugs used 0.1 mg/mL) using the above-mentioned procedure. For release purposes, the dual drug-loaded GPNM solution was dialyzed against acidic (pH 2) and basic (pH 7.4) medium. The release was monitored by taking UV−vis absorbance spectra at different time intervals.

RESULTS AND DISCUSSION

Spectral Characterization. Scheme 1 represents the synthesis protocol of GO-*g*-PNIPAM, by which different GPNM hybrids (GPNM 1:10, GPNM 1:50, GPNM 1:100;

DOI: 10.1021/am507110r
ACS Appl. Mater. Interfaces 2015, 7, 3512−3523

Supporting Information, Table S1) are synthesized using a simple in situ free radical polymerization technique. The successful grafting of monomer from GO sheets is manifested from ^{1}H NMR spectroscopic study. Figure S1a–c exhibits the NMR spectra of different GPNM samples in D_2O, and from the spectra it is clearly evident that NIPAM is polymerized from GO surface, as they show strong proton signals of PNIPAM units marked in the figure.

Raman spectroscopy is an important and nondestructive tool to characterize the electronic structure of carbon-based samples, and it is often used to study the structural changes of GO during chemical functionalization. Figure 1 exhibits the typical Raman spectra of GO and GPNM hybrids.

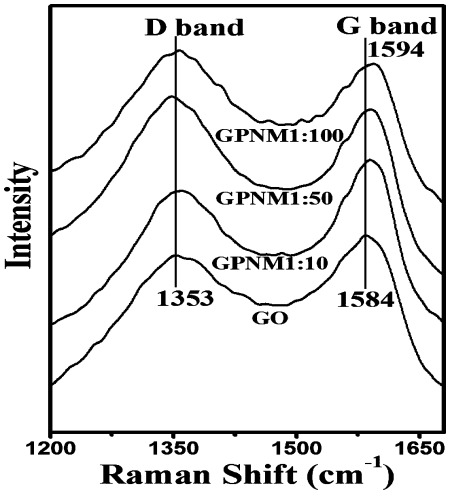

Figure 1. Raman spectra of GO and GPNM hybrids with indicated composition, where D and G denote the characteristic D and G bands of graphene.

The Raman spectrum of GO shows two prominent well-documented peaks at 1353 and 1584 cm^{-1}. The band at 1353 cm^{-1} is assigned to the D band, which arises due to the vibration of carbon atoms of disordered graphite, indicating the formation of sp^3 carbon in GO, whereas the band at 1584 cm^{-1} is allocated to the G band, which is associated with the first-order scattering of E_{2g} vibration mode for sp^2 carbon lattice of graphitic domain.[58] The G band in all the GPNM hybrids exhibits a gradual blue shift from 1584 cm^{-1}, and the blue shift becomes prominent (10 cm^{-1}) for GPNM 1:100 hybrid. The blue shift may be attributed to the tethering of PNIPAM chain on GO sheet via free radical process of grafting, deteriorating the alternate pattern of single–double bonds within the sp^2 carbon sheets. Furthermore, compared with GO the I_D/I_G intensity ratio of GPNM hybrids gradually enhances with increase of PNIPAM concentration (Table 1), indicating the gradual increase of sp^3 carbon structure after polymer grafting. We also calculated the size of sp^2 carbon clusters of GO and GPNM hybrids (Table 1) by employing Knight's empirical formula[59] on the Raman spectra.

$$L_a = 4.35/(I_D/I_G)$$

where L_a is designated as the size of sp^2 carbon clusters, and I_D/I_G is the intensity ratio between D and G band. From Table 1 it is confirmed that the grafting of PNIPAM from GO sheets causes a gradual reduction of graphitic structure causing an increase of I_D/I_G ratio and also decreasing the size of the graphitic domains with increase of NIPAM concentration in the GPNM systems.

Table 1. I_D/I_G Ratio and Crystalline Size of GO and GPNM Hybrids

sample name	I_D/I_G ratio	L_a (nm)
GO	0.91	4.78
GPNM1:10	0.95	4.58
GPNM1:50	1.01	4.30
GPNM1:100	1.05	4.14

A comparison of FTIR spectra of GO and GPNM hybrids further provides information about the attachment of PNIPAM to the surface of GO sheets (Supporting Information, Figure S2a). In case of GO the absorbance peaks at 1052, 1229, 1376, 1611, and 1710 cm^{-1} are attributed to the C–O stretching (alkoxy), asymmetric stretching modes of the epoxy (C–O–C) group, O–H stretching (carboxyl), C=C stretching (assigned to skeletal vibrations of unoxidized graphite domains), the stretching mode of carbonyl (C=O) bonds in both ketone and carboxylic acid groups, respectively.[57] The grafting of monomer from the GO surface introduces several new peaks clearly due to the incorporation of PNIPAM in the products. For instance, the band at 1557 cm^{-1} represents deformation of N–H band, whereas the band at 1650 cm^{-1} corresponds to the stretching vibrations of C=O band (amide I band), which can be ascribed to the typical vibration of O=CNH functionalities of PNIPAM segment. The amide I band shifts slightly to higher wavenumber (1650 cm^{-1}) from 1642 cm^{-1} of pure PNIPAM (Supporting Information, Figure S2b) due to the hydrogen bonding between >C=O groups of polymer molecules and GO sheets. Again, the prominent FTIR band at 1462 cm^{-1} corresponds to the isopropyl group of PNIPAM, which clearly proves the existence of PNIPAM on the surface of GO.

To obtain better insight into the surface functionalization from GO we performed the XPS spectroscopic study for GO and one of the hybrids (GPNM 1:50). The XPS spectrum of GO (Supporting Information, Figure S3) clearly indicates the presence of oxygen-containing functional groups after chemical oxidation of graphite powder. The survey scan XPS spectrum of the GPNM hybrid is depicted in Figure 2. In this spectrum, the peaks at 287, 401.2, and 532.9 eV correspond to C 1s, N 1s, and O 1s core level, respectively. The presence of N atoms of PNIPAM segment in the hybrid is distinctly identified by the XPS spectrum, presented in the inset of Figure 2, which confirms the grafting of PNIPAM from GO surface.

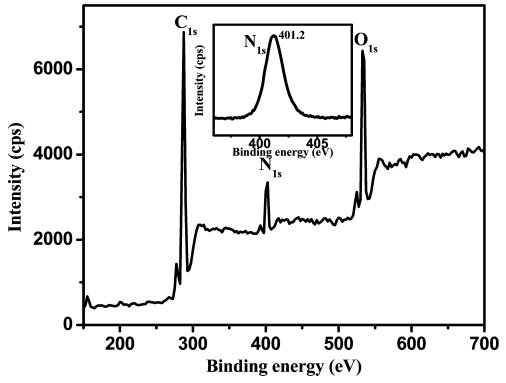

Figure 2. Survey scans XPS spectrum of GPNM 1:50. (inset) N 1s spectrum.

DOI: 10.1021/am507110r
ACS Appl. Mater. Interfaces 2015, 7, 3512–3523

Thermal Analysis. The thermal stability of GO and GPNM samples is determined from TGA thermograms (Supporting Information, Figure S4), and it is evident from Figure S4 that GO is not thermally stable since it starts decomposition below 100 °C due to the volatilization of adsorbed water in its π-stacked structure; the main mass loss occurs at ∼150−250 °C because of the pyrolysis of labile oxygen-containing groups such as −OH, −COOH, and epoxy groups.[60] On the contrary, after polymer grafting the stability of graphene sheets increases, and for GPNM hybrids the maximum mass loss occurs at ∼360 °C, which may be ascribed to the decomposition of the grafted PNIPAM chains. From the TGA thermogram it is important to note that the loss of oxygenous moiety in GPNM is prevented due to the wrapping of GO sheets with the PNIPAM chains that act as an effective shield prohibiting the heat flow.

Morphological Study. TEM is a useful tool to visually characterize the morphology of polymer-functionalized GO/graphene. Figure 3a,b and Supporting Information, Figure S5a,b exhibit the TEM images of GO and GPNM hybrids. The TEM image (Figure 3a) indicates the exfoliated sheet of GO, exhibiting clearly the smooth surface of GO sheet. The black patches over the sheets [Figure 3b and Supporting Information, Figure S5a,b] clearly imply the formation of PNIPAM from the GO surface.

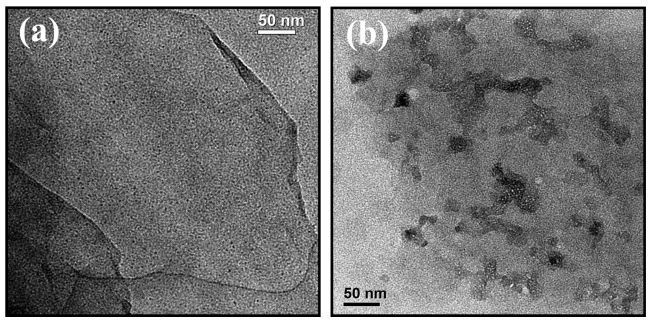

Figure 3. TEM images of (a) GO and (b) GPNM1:50 hybrid.

We further characterized the synthesized GPNM material by AFM [Figure 4a,b] to measure the thickness of the polymer grafted on GO sheets. From the height profile the thickness of GO sheets is found to be 0.85 nm, clearly suggesting almost a complete exfoliation of GO sheets. In contrast, on polymerization with NIPAM the thickness of GPNM has increased to 3.2 nm indicating that the PNIPAM chains are successfully grafted from the surfaces of GO sheets.

Spectral Properties. Fluorescence in amorphous carbon-based materials arises due to the radiative recombination of electrons and holes (e−h) created by confined sp^2 clusters.[61] The sp^2 clusters in heterogeneous carbon network like GO have opened up electronic band gaps, which are inherently associated with their sizes, shapes, and fractions as well as the symmetry and topology of the sp^2 chains and clusters.[62] The fluorescence spectra of GO and GPNM hybrid solutions (aqueous) are presented in Figure 5, and from the spectra it is quite evident that GO shows very weak emission at 443 nm due to the presence of epoxy, carboxyl, and hydroxyl groups causing a greater proportion of nonradiative decay of excitons. On the contrary, after grafting of PNIPAM from the GO surface the fluorescence intensity dramatically increases with an increase of NIPAM weight ratio with a gradual blue shift of the emission peak.

To obtain a vivid idea about the origin of enhanced fluorescence property of the GPNM hybrids the sp^2 cluster sizes of GO and GPNM hybrids (Table 1) are considered, and

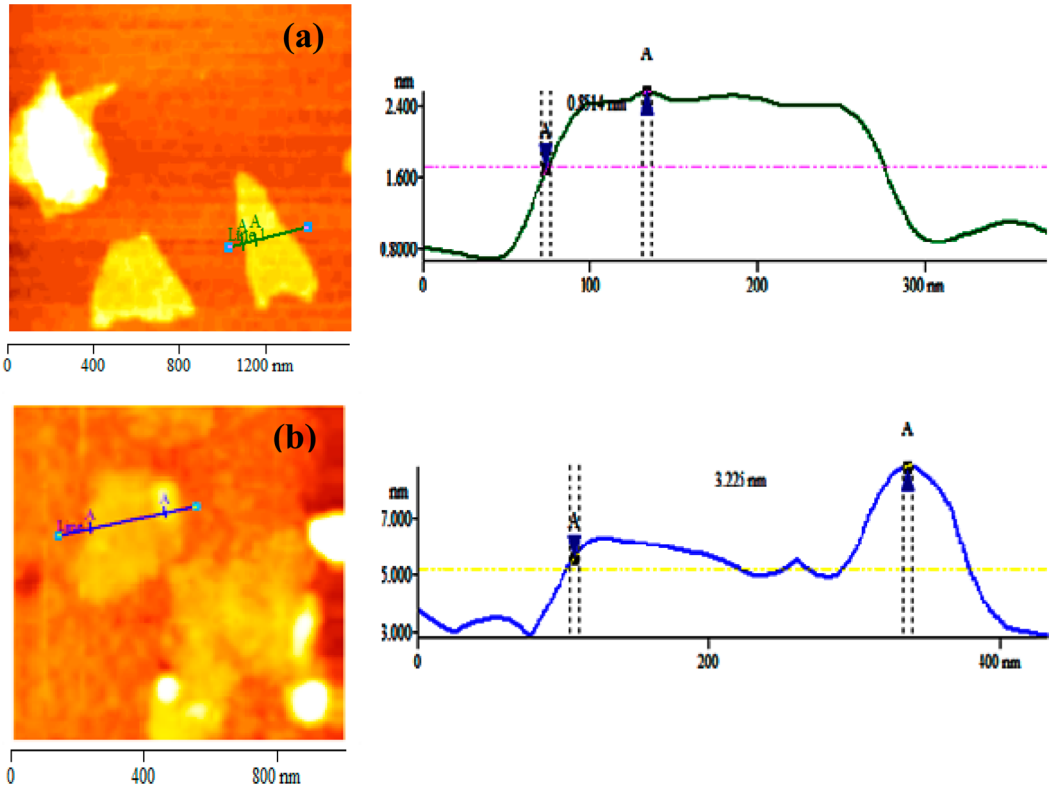

Figure 4. Tapping mode AFM images and height profile of (a) GO and (b) GPNM1:50.

DOI: 10.1021/am507110r
ACS Appl. Mater. Interfaces 2015, 7, 3512−3523

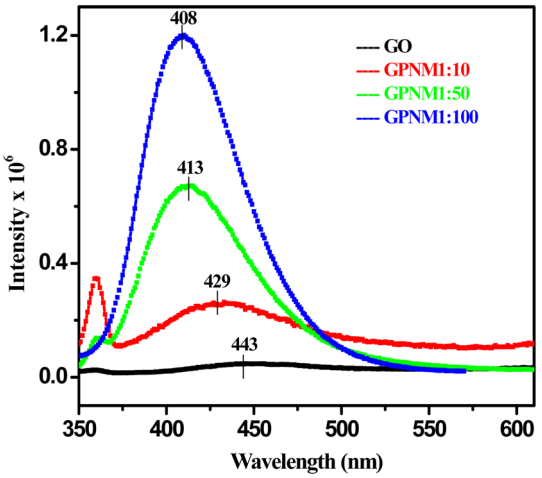

Figure 5. Fluorescence spectra of GO and GPNM hybrids with indicated composition for excitation at 320 nm.

cluster size varies in the range of 4.78 to 4.14 nm. The size of sp^2 clusters of GO is ~4.8 nm, which may account for the weak blue emission of GO, though different propositions are put forwarded in recent reports.[20−24] Pan et al.[63] have suggested that the blue emission of GO might originate from the free zigzag sites with a carbene-like triplet $\sigma^1\pi^1$ground state. In contrast the creation of smaller sp^2 clusters and structural defects during the polymerization process are likely to be responsible for the origination and augmentation of blue emission for all the GPNM hybrids. From Figure 5 it is quite obvious that there is a gradual blue shift of the emission peak in all the hybrids with increase in PNIPAM concentration from that of GO. This may be attributed to the lowering of sp^2 domain size, defect level transition, and structural changes, since it is well-documented that both the structure and defects influence the electronic structure of nanomaterials, changing their optical properties appreciably.[64] Again, the grafting of PNIPAM from the GO surface results in a reduction of GO planarity (as reflected from the I_D/I_G values, Table 1) resulting in a less-conjugated system where the nonradiative hopping of excitons would be restricted causing both an enhancement in fluorescence intensity and a blue shift of the emission peak of the hybrids.

Owing to the incorporation of PNIPAM, the polymer-grafted GO sheets become readily dissolved in water under sonication, and the dispersion remains stable for months. At room temperature (25 °C) the >C═O and N−H bonds of PNIPAM form intermolecular hydrogen bonds with the surrounding solvent (water) molecules, which limits the motion of bound water molecules. This phenomenon prevents the aggregation of GO sheets; thus, the interlayer quenching and the dynamic quenching of fluorescence intensity due to the smaller solvent (bulk water) molecules are reduced to a great extent.[33] These aforementioned factors cause the passivation of GO surface due to the polymerization of NIPAM, which certainly contributes to the enhancement of fluorescence intensity of all the GPNM hybrids where the degree of enhancement depends on the degree of passivation.

The fluorescence study of the GPNM hybrids at pH 4 and 9.2 are presented in Supporting Information, Figure S6a,b, and the same trend of fluorescence intensity enhancement with increase of NIPAM concentration exists in all these pH, suggesting that the above reasons behind the augmentation of fluorescence intensity are legitimate. In Supporting Information, Figure S7a, a comparison of fluorescence intensity enhancement with NIPAM concentration at different pH is presented, and it is clear that at pH 4 the fluorescence intensity and its increase rate is higher than those at other pH. A probable reason is that the protonation of carboxyl and epoxy groups of GO/GPNM hybrid reduces the accessibility of nonbonding electrons responsible for nonradiative recombination of holes of GO significantly, causing an increase of the emission intensity. At higher pH values (pH 7 and pH 9.2) ionization of carboxylic acid groups causes an increase of the accessibility of electrons responsible for nonradiative recombination of holes of GO yielding lower fluorescence intensity than that at pH 4.[28,33,34] It is necessary to mention here that to utilize this system for biological applications the fluorescence property at pH 7 is certainly important as most of the biological processes occur at these pH. In Supporting Information, Figure S7b the wavelength of emission peak is plotted with NIPAM concentration in the GPNM hybrids at different pH. It is interesting to note that in all the pH there is a gradual blue shift of the emission peak with rise of NIPAM concentration, and this is attributed to the increased disorder of the graphitic structure (Table 1) due to grafting of higher amount of NIPAM on the GO surface. Again, with increase of pH for every system the blue shift increases due to the increase in the band gap at higher pH for ionization of −COOH and −OH groups causing electrostatic doping,[65] which also elevates the disorder of GO to higher extent.

We also performed the temperature-dependent fluorescence property of both GO and GPNM hybrid. The fluorescence spectrum of GO (presented in Supporting Information, Figure S8) is almost temperature-invariant. In contrast, the fluorescence spectra of GPNM 1:50 hybrid (Figure 6) depict a nice

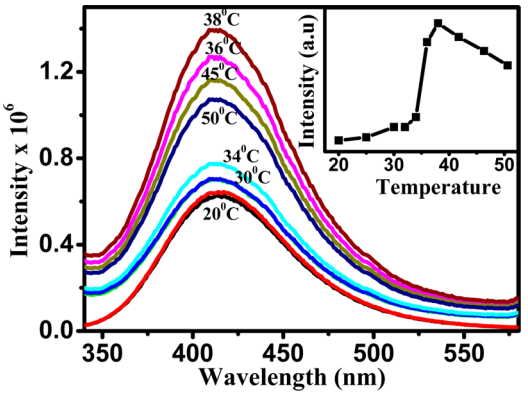

Figure 6. Temperature-dependent fluorescence spectra of GPNM 1:50 hybrid.

change of fluorescence intensity with temperature and show a sharp increase at 36 °C, and this may be attributed to the phase separation of PNIPAM chains above its LCST causing the formation of different microenvironment (hydrophobic), which reduces the quenching of excitons of GO by solvent molecules (water) to some extent. Above LCST the whole system remains as turbid dispersion, which does not allow collapsed PNIPAM chains sufficiently closer to GO sheets probably due to the steric hindrance created by the tethered segments and the oxygen-containing groups anchored from the GO surface prohibiting the rest part of the grafted PNIPAM chains to collapse on the GO surface. The aggregation of PNIPAM

DOI: 10.1021/am507110r
ACS Appl. Mater. Interfaces 2015, 7, 3512−3523

chains within themselves above the tethered segments keeps the GO as a core that protects the quenching of GO excitons with the water molecules. A small decrease of fluorescence intensity above LCST in the GPNM sample may be attributed to quenching that occurs from the intermolecular exciton transfer in the GPNM-rich phase. PNIPAM itself has no fluorescence property, but the substantial fluorescence property of GPNM hybrid encourages its use as a thermoresponsive fluorescent material.

For a comparison of the thermoresponsiveness of PNIPAM and GPNM hybrid the temperature-dependent absorbance was studied. The temperature-dependent absorbance of PNIPAM [Supporting Information, Figure S9a] shows a sudden jump at 32 °C, whereas GPNM [Supporting Information, Figure S9b] displays a sharp change of absorbance at 37 °C. The LCST of PNIPAM appears because of the breaking of H-bonds with the water (solvent) molecules facilitating the interchain aggregation. On the contrary, in GPNM system the attachment of GO sheet with PNIPAM hinders the aggregation process due to the −OH, −COOH, and epoxy groups, which favor the GPNM system to remain as aqueous dispersion. The steric hindrance of the attached graphitic domain may also prevent the interchain aggregation of PNIPAM at least to some extent contributing to the increase of LCST of the GPNM system.

Biomedical Application. To appraise the potential application of GPNM hybrids in the biomedical field by exploiting their excellent hydrophilic, fluorescence, and drug-loading (discussed below) properties, their biocompatibility with U87MG and 3T3-L1 cells were determined. The differential interference contrast microscopy (DIC) images of U87MG and 3T3-L1 cells incubated into different material with final concentration of 17 μg/mL are depicted in Supporting Information, Figures S10 and S11, respectively. The DIC images clearly demonstrate that the cells still keep their normal morphology after 24 h incubation with GPNM (Supporting Information, Figures S10c and S11c). Similarly, GO also shows good biocompatibility at the same final concentration after 24 h. To further confirm the excellent biocompatibility of GPNM, in vitro cytotoxicity effect of GO and as-synthesized GPNM hybrid was investigated by conventional MTT assay using U87MG and 3T3-L1 cells. GO and GPNM hybrid solutions of different concentration were incubated with the cells for 24 h, then standard MTT assay was performed to determine the relative cell viability assuming 100% viability for cells without any materials. The cell viability of GO and GPNM hybrid solutions with U87MG and 3T3-L1 cells are presented in Figures 7 and 8, respectively. No significant change in cell viability is observed when cells were incubated with GPNM solution having concentration of 2−100 μg/mL for 24 h. At higher concentration the cell viability of GPNM is found to be ∼80% for both kinds of cells. The cell viability of GO at low concentrations is similar to GPNM, but it significantly reduces at higher concentrations for both of the systems.

Thus, the cell viability measurement of GPNM from both cancer and normal cell lines confirms the excellent biocompatibility. It is necessary to mention here that in GPNM the actual amount of GO is lower than GO at the same concentration of analyte (w/v), and the cell viability data are not normalized with respect to GO concentration. The main aim of functionalization is to get improved biocompatibility for the same analyte concentration to visualize the effect of synthesized material. The functionalization of GO with PNIPAM therefore

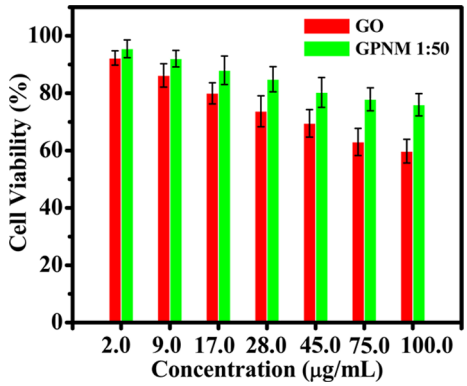

Figure 7. Relative cell viability of U87MG cells after 24 h of incubation with GO and GPNM hybrid solution; error bars are based on three repetitive measurements.

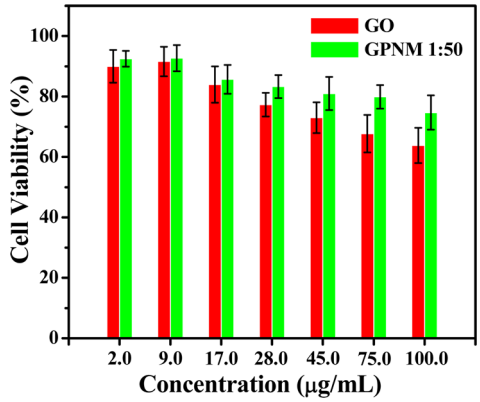

Figure 8. Relative cell viability of 3T3-L1 cells after 24 h of incubation with GO and GPNM hybrid solution; error bars are based on three repetitive measurements.

yields more biocompatibility and dispersibility in cell medium preventing aggregation of GO sheets.

In view of their excellent optical properties and biocompatibility, GPNM has great prospects for biomedical applications. Hence, we used this biocompatible nanomaterial for the loading and release of DOX (a well-known hydrophilic anticancer drug extensively used in chemotherapy). For that purpose, we first studied the effect of free DOX and GPNM-DOX on the cell morphology using DIC microscopy (Supporting Information, Figure S12). Again, to affirm whether GPNM could carry DOX readily into cells, we investigated the cellular uptake of DOX and GPNM-DOX by U87MG cells after 6 h of incubation (final DOX concentration is 8.5 μg/mL) through both optical and fluorescence imaging. As shown in Figure 9, fluorescence is observed in U87MG cells for both free drug and drug-loaded GPNM hybrid, which clearly demonstrates the delivery of drug into the cells via penetrating cell membranes. To further confirm that DOX-loaded GPNM hybrid is really taken up by the cell and not by the free DOX in cell culture medium, U87MG cells were incubated with GPNM-DOX for 30 min and additional 5 h incubation with fresh DMEM medium after washing. Fluorescence imaging study (Supporting Information, Figure S13) shows that after 30 min very low fluorescence signal of DOX into the cells is observed due to the low uptake of GPNM-DOX hybrid. If free DOX exists, better fluorescence imaging would be observed. After additional incubation of 5 h

DOI: 10.1021/am507110r
ACS Appl. Mater. Interfaces 2015, 7, 3512−3523

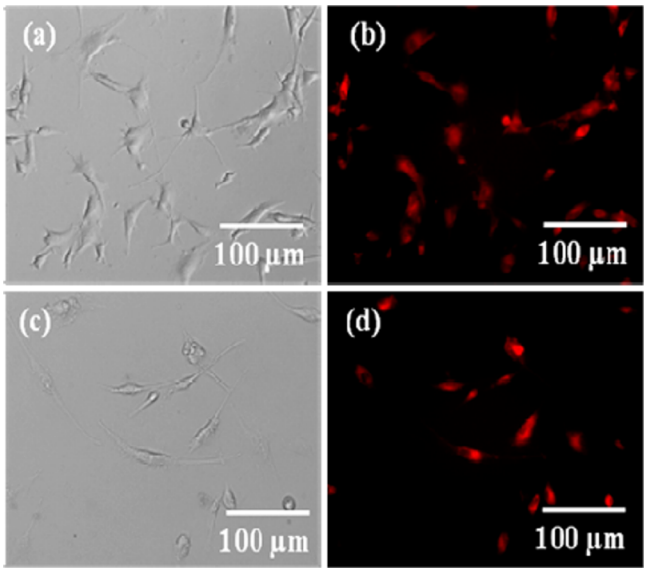

Figure 9. Cellular uptake of free DOX (a, b) and DOX-loaded GPNM hybrid (c, d) by U87MG cells after 6 h of incubation. The images of live cells were taken in differential interference contrast mode (a, c) and fluorescence mode (b, d).

the fluorescence signal of DOX into cells increased because of the release of DOX from GPNM-DOX in the cell.

The cytotoxicity effects of DOX and GPNM-DOX are also measured via MTT-based assay using U87MG cells. Figure 10

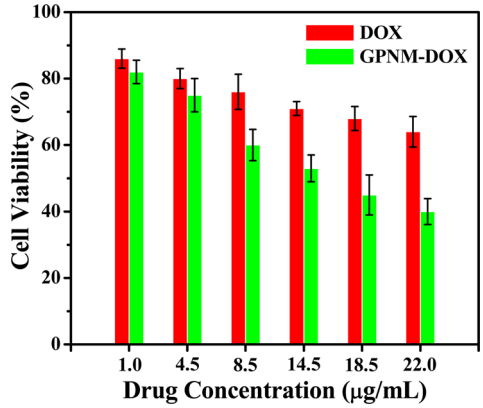

Figure 10. Relative cell viability of U87MG cells after 24 h of incubation with DOX and GPNM-DOX solution with varying concentration of DOX; error bars are based on three repetitive measurements.

shows the relative cell viability of U87MG cells after incubating with DOX and GPNM-DOX for 24 h while varying the concentration of DOX. The result clearly indicates that GPNM-DOX exhibits higher cytotoxic effect compared to free drug with increasing drug concentration. Thus, obviously GPNM can carry DOX into cells to improve the drug efficiency compared to DOX without GPNM.

Now, we monitored the loading and release of DOX through different spectroscopic techniques. The DOX-loaded GPNM (GPNM-DOX) becomes readily dispersed in water, forming a clear transparent solution with reddish color. The loading of DOX was monitored by both UV−vis and fluorescence spectroscopic investigations. The UV−vis absorption spectra of different GPNM-DOX solutions with the same GPNM concentration (0.2 mg/mL) but variable DOX concentration evidently represent the appearance of characteristic DOX absorbance peaks (Supporting Information, Figure S14) testifying to the successful loading of DOX onto the GPNM hybrid even after three times washing of GPNM-DOX samples with water. The actual concentration of DOX loaded onto GPNM (Supporting Information, Table S2) is measured by the absorbance peak of DOX after subtracting the absorbance of GPNM solution at the same wavelength, and the calibration plot is also shown in Supporting Information, Figure S15 (inset). The fluorescence spectra of free DOX and GPNM-DOX with different DOX concentration but for the same GPNM concentration (0.2 mg/mL) at pH 7.4 are shown in Supporting Information, Figure S16. As evidenced from Figure S16, a significant quenching of DOX fluorescence upon binding onto GPNM surface is observed, indicating the closer proximity of DOX molecules to the graphene surface.[66] Again the loading of DOX molecules with the same DOX concentration but different GPNM concentration (0.1 mg/mL to 0.3 mg/mL) is also evidenced from fluorescence spectra presented in Supporting Information, Figure S17. The fluorescence spectra clearly indicate that DOX fluorescence intensity gradually decreases with increase of GPNM concentration from 0.1 to 0.3 mg/mL. Thus, obviously GPNM plays a definite role for binding of DOX onto its surface through noncovalent interaction driven by $\pi-\pi$ stacking, hydrophobic, and hydrogen bonding interactions.[67] With GO−DOX system the same type of interactions are possible, but a major difficulty is that the GO−DOX system does not form stable dispersion, since GO is not so much stable either in physiological condition or in the cell culture media, as evidenced from the digital photographs (Supporting Information, Figures S18 and S19). Thus, our synthesized material can serve as better nanomaterial for the in vitro application than GO alone.

For our study we selected the GPNM-DOX sample with lowest DOX concentration having the GPNM concentration of 0.2 mg/mL, and for clarity the fluorescence spectra of free DOX and GPNM-DOX at the same DOX concentration is shown in Figure 11. The loading capacity of drug is calculated

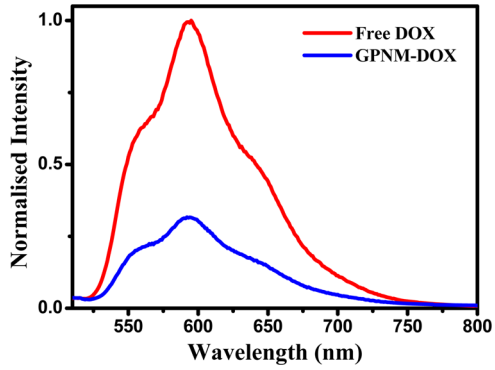

Figure 11. Fluorescence spectra of free DOX and GPNM-DOX at the same DOX concentration under 490 nm excitation.

by monitoring the emission peak intensity of the drug at 595 nm with the help of following equation:

$$\text{loading capacity} = 100 - \{(\text{DOX intensity in presence of GPNM})/(\text{free DOX intensity}) \times 100\}$$

DOI: 10.1021/am507110r
ACS Appl. Mater. Interfaces 2015, 7, 3512−3523

The loading capacity is determined to be 71, 78, and 83% for the increase in GPNM concentration from 0.1 to 0.3 mg/mL at the same DOX concentration.

The release of DOX from GPNM hybrid is carried out by changing the chemical environment to acidic. For that purpose the DOX-loaded GPNM (GPNM-DOX1) is incubated at pH 4 buffer solutions, and the released DOX from GPNM surface is monitored by fluorescence spectroscopy using the supernatant of GPNM-DOX1 sample at different time intervals after centrifugation. The release of DOX at different time intervals is substantiated from the gradual increased fluorescence intensity of GPNM-DOX1 sample with passage of time (Figure 12 and Supporting Information, Figure S20) indicating that the release of DOX from GPNM surface is pH-triggered.

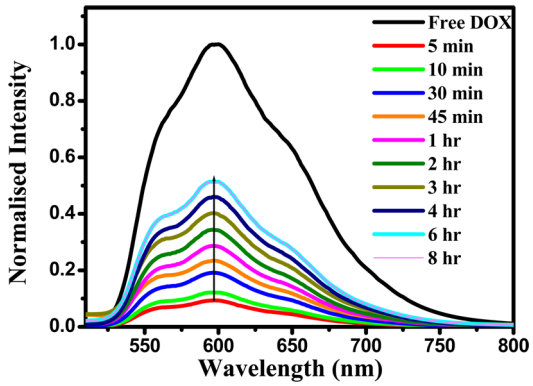

Figure 12. Release of DOX from GPNM-DOX1 sample at pH 4.

This phenomenon of drug release might be attributed to the protonation of amino group in the DOX molecule at lower pH, which renders enhanced hydrophilicity and higher solubility to DOX, minimizing the hydrogen bonding interaction between DOX and GPNM surface.[67] The aforementioned observations reveal that DOX is bound to the surface of GPNM at normal physiological condition but released at lower pH (pH 4) similar to the microenvironments of extracellular tissues of tumors, intracellular lysosomes and endosomes, or cancerous tissue. Thus, this pH-triggered drug release from GPNM hybrid could be exploited for site-specific drug delivery.

We further loaded practically water-insoluble, nonsteroidal anti-inflammatory drug IMC on the surface of GPNM hybrid via noncovalent interaction between IMC and GPNM, thus improving the stability of the drug in aqueous medium. This widely used drug has an important role in the treatment of soft-tissue problems associated with trauma, osteoarthritis, ankylosing spondylitis, rheumatoid arthritis, and acute gouty arthritis by suppressing prostaglandin synthesis in the tissues via inhibition of cyclooxygenase activity.[68] Poor water solubility of IMC has restricted its application for oral administration.

To overcome this problem we tried to enhance the water solubility of IMC using our biocompatible GPNM hybrid. The loading of IMC on the surface of GPNM hybrid is evident from the UV–vis spectra (Figure 13). The appearance of characteristic peak of IMC at 319 nm in all the GPNM-IMC samples clearly reveals the successful loading of IMC on the surface of GPNM hybrid.

Further we investigated the pH-dependent release behavior of IMC using alginate-encapsulated GPNM–IMC beads to understand the real applicability of our designed system as a potent carrier of IMC in oral delivery. Since oral delivery must

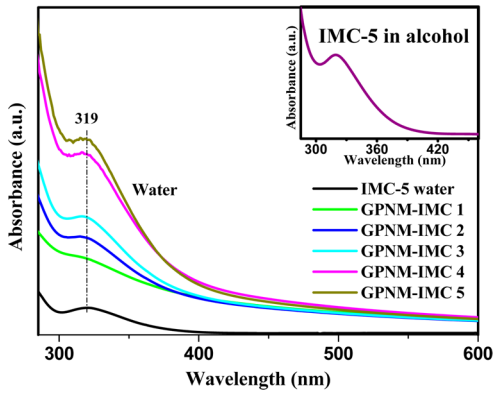

Figure 13. UV–vis absorbance spectra of free IMC in alcohol (inset) and GPNM-IMC in water at the same GPNM concentration (0.2 mg/mL) but different IMC concentration (IMC 1 to IMC 5).

tolerate both acidic environment in stomach (pH of gastric juice: 1.2–2) and basic surroundings in intestine (pH of intestinal juice: 7.4), here we studied the release behavior of the drug at pH 2 and 7.4 using UV–vis spectroscopy (Figure 14).

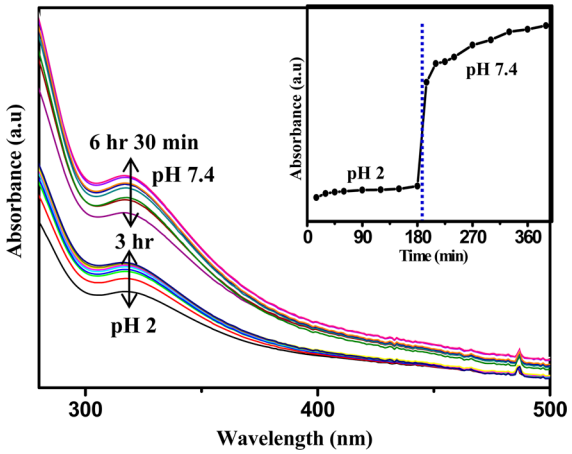

Figure 14. pH-dependent release of IMC from alginate-encapsulated GPNM–IMC beads using UV–vis spectra. (inset) Release profiles at pH 2 and pH 7.4.

It is quite obvious from the UV–vis spectra that drug release at pH 7.4 is more prominent than at pH 2 due to the higher solubility of IMC at pH 7.4,[69] which permits better diffusion of the drug from alginate-encapsulated GPNM–IMC beads. This encapsulation technique using GPNM as a nontoxic material may allow the oral delivery of IMC while suppressing side effects such as irritation of gastrointestinal mucosa due to direct exposure of IMC.[68]

Moreover IMC can bind with HSA, which is the major transport protein of the mammalian blood circulation.[70] This phenomenon assisted us in the design of a new biocompatible material that can serve as a carrier of IMC. Since IMC has strong affinity to HSA, we thought that our nanocarrier may be used for the transport of IMC following the releasing ability to HSA.

The release of IMC from GPNM surface is revealed in Figure 15. Only HSA shows characteristic UV–vis peak at 278 nm (Figure 15 inset). But, upon release of IMC from GPNM surface, a new peak at 319 nm appears, which supports the presence of IMC in the dialysate. Thus, the UV–vis spectra

DOI: 10.1021/am507110r
ACS Appl. Mater. Interfaces 2015, 7, 3512–3523

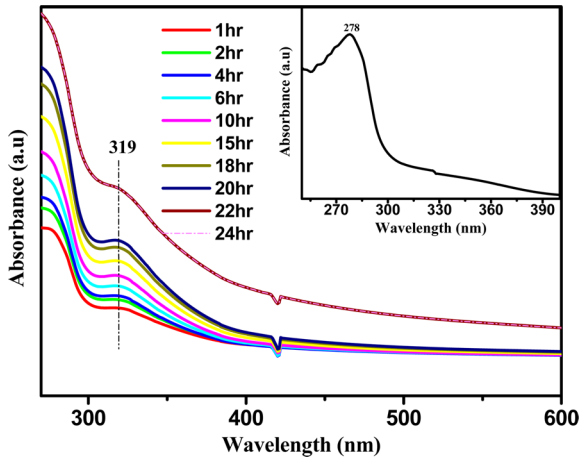

Figure 15. Release of indomethacin from GPNM surface monitored by UV−vis spectra (inset) UV−vis spectrum of HSA.

clearly reveal the potential of our synthesized nanomaterial as a hydrophobic drug-delivery vehicle.

We also studied the possibility of simultaneous drug delivery using GPNM nanocarrier though the drugs are used for different clinical functions. For that purpose, we used the previously stored GPNM-DOX solution to load the hydrophobic drug IMC according to the aforementioned procedure. The UV−vis spectrum (Supporting Information, Figure S21) exhibited the characteristic absorbance peaks both of IMC (at 315 nm) and DOX (at 501 nm), suggesting the simultaneous loading of both of the drugs. For the study of simultaneous release phenomenon, the dual drug-loaded GPNM solution was dialyzed against acidic (pH 2) and basic (pH 7.4) medium, and the release of both the drugs was monitored by taking the absorbance spectra of the dialysate at different time intervals. The UV−vis spectra depicted in Figure 16 clearly reveals that

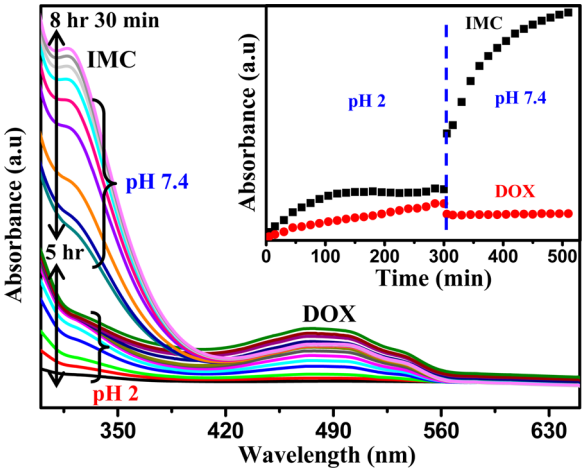

Figure 16. Simultaneous release of DOX and IMC from GPNM surface in acidic and basic medium monitored by UV−vis spectra (inset) Release profiles of DOX and IMC at different pH.

both of the drugs released at pH 2, but at higher pH the release of IMC is more prominent, and that DOX exhibits a negligible release (inset, Figure 16). Thus, we believe that our nanocarrier may be used for simultaneous drug-delivery purposes.

CONCLUSIONS

In summary, we have successfully demonstrated a facile, cost-effective, and efficient approach to graft PNIPAM to GO surface using a simple in situ FRP technique. The GPNM hybrid furnishes high dispersibility and stability to graphene sheets in aqueous as well as cell media. The thermal stability of GPNM is highly enhanced compared to that of GO. As-synthesized GPNM hybrids exhibit interesting fluorescence property in aqueous medium along with a temperature-dependent fluorescence property with a sudden jump of fluorescence intensity at 36 °C for the phase separation of PNIPAM chains above its LCST (32 °C). Furthermore, the GPNM hybrid displays good biocompatibility and is proven to be practically nontoxic. Owing to its $\pi-\pi$ stacking, H-bonding, and hydrophobic interactions, GPNM hybrid acquires superior potential for binding both hydrophilic and hydrophobic aromatic drugs. The release of the hydrophilic anticancer drug DOX has been accomplished at pH 4, which is relevant to the environment of cancer cells. Furthermore, cellular uptake and MTT-based assay study unveils that the efficiency of drug is improved after loading. On the other hand, the hydrophobic drug IMC also exhibits pH-dependent release as well as release to HSA. Additionally, GPNM is found to be a potential nanocarrier for simultaneous delivery of both the hydrophilic and hydrophobic drugs. Thus, the present study reveals that in view of its excellent properties like high dispersibility, thermoresponsive fluorescence property, good biocompatibility, and stability in aqueous solution at physiological condition, GPNM has great prospects as a promising nanomaterial for a wide range of biomedical applications such as simultaneous drug delivery, controlled release, cell imaging, etc.

ASSOCIATED CONTENT

Supporting Information

Table for preparation of GPNM samples; ^{1}H NMR spectra of different GPNM systems; FTIR spectra of GO, GPNM samples, and pure PNIPAM; XPS spectrum of GO; TGA curves of GO and GPNM 1:50; TEM images of GPNM 1:10 and GPNM 1:100 systems; fluorescence spectra of GO and different GPNM hybrids at pH 4 and pH 9.2; plot of fluorescence intensity and wavelength versus composition at different pH; temperature-dependent fluorescence spectra of GO and absorbance spectra of pure PNIPAM and GPNM 1:50 hybrid in water; DIC images of 3T3-L1 cells in the presence of GO and GPNM and U87MG cells in the presence of GO, GPNM, DOX, and GPNM-DOX; DIC and fluorescence images of U87MG cells in the presence of GPNM-DOX with low incubation time; UV−vis absorbance spectra of free DOX with various concentrations and corresponding calibration curve; table for the loaded amount of DOX in different GPNM-DOX samples; fluorescence spectra of free DOX and GPNM-DOX with different DOX concentrations at the same GPNM concentration; fluorescence spectra of free DOX at pH 7.4 and GPNM-DOX at the same DOX concentration with different GPNM concentrations; digital photographs; UV−vis absorbance spectra of free DOX and GPNM-DOX at the same GPNM concentration with different DOX concentrations; release profile of DOX at pH 4; UV−vis absorbance spectrum for simultaneous loading of drugs. This material is available free of charge via the Internet at http://pubs.acs.org.

DOI: 10.1021/am507110r
ACS Appl. Mater. Interfaces 2015, 7, 3512−3523

AUTHOR INFORMATION

Corresponding Author

*E-mail: psuakn@iacs.res.in. Fax: (+91) 33 2473 2805.

Present Address

‡CAM, I.A.C.S., Jadavpur, Kolkata 700032, India.

Notes

The authors declare no competing financial interest.

ACKNOWLEDGMENTS

We gratefully acknowledge CSIR (Grant No. 02(0051)/12/EMR-II), New Delhi, and DST Unit of Nanoscience at IACS for financial support. A.K., S.N., and P.D. gratefully acknowledge CSIR, New Delhi, for providing fellowship. We acknowledge Dr. N. R. Jana of CAM, IACS, for helping in cellular study. We also like to acknowledge Prof. M. Ray of Bose Institute, Kolkata, for providing the drugs.

REFERENCES

(1) Allen, M. J.; Tung, V. C.; Kaner, R. B. Honeycomb Carbon: A Review of Graphene. *Chem. Rev.* **2010**, *110*, 132−145.

(2) Zhang, C.; Ren, L.; Wang, X.; Liu, T. Graphene Oxide-Assisted Dispersion of Pristine Multiwalled Carbon Nanotubes in Aqueous Media. *J. Phys. Chem. C* **2010**, *114*, 11435−11440.

(3) Dreyer, D. R.; Park, S.; Bielawski, C. W.; Ruoff, R. S. The Chemistry of Graphene Oxide. *Chem. Soc. Rev.* **2010**, *39*, 228−240.

(4) Navarro, C. G.; Burghard, M.; Kern, K. Elastic Properties of Chemically Derived Single Graphene Sheets. *Nano Lett.* **2008**, *8*, 2045−2049.

(5) Zhao, X.; Zhang, Q.; Chen, D.; Lu, P. Enhanced Mechanical Properties of Graphene-Based Poly(vinyl alcohol) Composites. *Macromolecules* **2010**, *43*, 2357−2363.

(6) Dikin, D. A.; Stankovich, S.; Zimney, E. J.; Piner, R. D.; Dommett, G. H. B.; Evmenenko, G.; Nguyen, S. T.; Ruoff, R. S. Preparation and Characterization of Graphene Oxide Paper. *Nature* **2007**, *448*, 457−460.

(7) Yang, W.; Ratinac, K. R.; Ringer, S. P.; Thordarson, P.; Gooding, J. J.; Braet, F. Carbon Nanomaterials in Biosensors: Should You Use Nanotubes or Graphene? *Angew. Chem., Int. Ed.* **2010**, *49*, 2114−2138.

(8) Zhu, Y.; James, D. K.; Tour, J. M. New Routes to Graphene, Graphene Oxide and Their Related Applications. *Adv. Mater.* **2012**, *24*, 4924−4955.

(9) Chen, D.; Feng, H.; Li, J. Graphene Oxide: Preparation, Functionalization, and Electrochemical Applications. *Chem. Rev.* **2012**, *112*, 6027−6053.

(10) Compton, O. C.; Nguyen, S. T. Graphene Oxide, Highly Reduced Graphene Oxide, and Graphene: Versatile Building Blocks for Carbon-Based Materials. *Small* **2010**, *6*, 711−723.

(11) Cai, W.; Piner, R. D.; Stadermann, F. J.; Park, S.; Shaibat, M. A.; Ishii, Y.; Yang, D.; Velamakanni, A.; An, S. J.; Stoller, M.; An, J.; Chen, D.; Ruoff, R. S. Synthesis and Solid-State NMR Structural Characterization of ^{13}C-Labeled Graphite Oxide. *Science* **2008**, *321*, 1815−1817.

(12) Yang, D.; Velamakanni, A.; Bozoklu, G.; Park, S.; Stoller, M.; Piner, R. D.; Stankovich, S.; Jung, I.; Field, D. A.; Ventricejr, C. A.; Ruoff, R. S. Chemical Analysis of Graphene Oxide Films after Heat and Chemical Treatments by X-ray Photoelectron and Micro-Raman Spectroscopy. *Carbon* **2009**, *47*, 145−152.

(13) Novoselov, K. S.; Geim, A. K.; Morozov, S. V.; Jiang, D.; Zhang, Y.; Dubonos, S. V.; Grigorieva, I. V.; Firsov, A. A. Electric Field Effect in Atomically Thin Carbon Films. *Science* **2004**, *306*, 666−669.

(14) Dai, L.; He, P.; Li, S. Functionalized Surfaces Based on Polymers and Carbon Nanotubes for Some Biomedical and Optoelectronic Applications. *Nanotechnology* **2003**, *14*, 1081−1097.

(15) Mohanty, N.; Berry, V. Graphene-Based Single-Bacterium Resolution Biodevice and DNA Transistor: Interfacing Graphene Derivatives with Nanoscale and Microscale Biocomponents. *Nano Lett.* **2008**, *8*, 4469−4476.

(16) Zuo, X.; He, S.; Li, D.; Peng, C.; Huang, Q.; Song, S.; Fan, C. Graphene Oxide-Facilitated Electron Transfer of Metalloproteins at Electrode Surfaces. *Langmuir* **2010**, *26*, 1936−1939.

(17) Mei, Q.; Zhang, K.; Guan, G.; Liu, B.; Wang, S.; Zhang, Z. Highly Efficient Photoluminescent Graphene Oxide with Tunable Surface Properties. *Chem. Commun.* **2010**, *46*, 7319−7321.

(18) Kuila, T.; Bhadra, S.; Yao, D.; Kim, N. H.; Bose, S.; Lee, J. H. Recent Advances in Graphene Based Polymer Composites. *Prog. Polym. Sci.* **2010**, *35*, 1350−1375.

(19) Scheuermann, G. M.; Rumi, L.; Steurer, P.; Bannwarth, W.; Mulhaupt, R. Palladium Nanoparticles on Graphite Oxide and Its Functionalized Graphene Derivatives as Highly Active Catalysts for the Suzuki-Miyaura Coupling Reaction. *J. Am. Chem. Soc.* **2009**, *131*, 8262−8270.

(20) Sun, X.; Liu, Z.; Welsher, K.; Robinson, J. T.; Goodwin, A.; Zaric, S.; Dai, H. Nano-Graphene Oxide for Cellular Imaging and Drug Delivery. *Nano Res.* **2008**, *1*, 203−212.

(21) Liu, Z.; Robinson, J. T.; Sun, X.; Dai, H. PEGylated Nanographene Oxide for Delivery of Water-Insoluble Cancer Drugs. *J. Am. Chem. Soc.* **2008**, *130*, 10876−10877.

(22) Fan, F. R. F.; Park, S.; Zhu, Y.; Ruoff, R. S.; Bard, A. J. Electrogenerated Chemiluminescence of Partially Oxidized Highly Oriented Pyrolytic Graphite Surfaces and of Graphene Oxide Nanoparticles. *J. Am. Chem. Soc.* **2008**, *131*, 937−939.

(23) Lu, C. H.; Yang, H. H.; Zhu, C. L.; Chen, X.; Chen, G. N. A Graphene Platform for Sensing Biomolecules. *Angew. Chem., Int. Ed.* **2009**, *48*, 4785−4787.

(24) Luo, Z.; Vora, P. M.; Mele, E. J.; Johnson, A. T. C.; Kikkawa, J. M. Photoluminescence and Band Gap Modulation in Graphene Oxide. *Appl. Phys. Lett.* **2009**, *94*, 111909.

(25) Zhang, X.-F.; Shao, X.; Liu, S. Dual Fluorescence of Graphene Oxide: A Time-Resolved Study. *J. Phys. Chem. A* **2012**, *116*, 7308−7313.

(26) Kozawa, D.; Miyauchi, Y.; Mouri, S.; Matsuda, K. Exploring the Origin of Blue and Ultraviolet Fluorescence in Graphene Oxide. *J. Phys. Chem. Lett.* **2013**, *4*, 2035−2040.

(27) Cao, L.; Meziani, M. J.; Sahu, S.; Sun, Y. P. Photoluminescence Properties of Graphene versus Other Carbon Nanomaterials. *Acc. Chem. Res.* **2013**, *46*, 171−180.

(28) Chen, J. L.; Yan, X. P. Ionic Strength and pH Reversible Response of Visible and Near-Infrared Fluorescence of Graphene Oxide Nanosheets for Monitoring the Extracellular pH. *Chem. Commun.* **2011**, *47*, 3135−3137.

(29) Galande, C.; Mohite, A. D.; Naumov, A. V.; Gao, W.; Ci, L.; Ajayan, A.; Gao, H.; Srivastava, A.; Weisman, R. B.; Ajayan, P. M. Quasi-Molecular Fluorescence from Graphene Oxide. *Sci. Rep.* **2011**, *1*, 1−5.

(30) Shang, J.; Ma, L.; Li, J.; Ai, W.; Yu, T.; Gurzadyan, G. G. The Origin of Fluorescence from Graphene Oxide. *Sci. Rep.* **2012**, *2*, 1−8.

(31) Chen, J. L.; Yan, X. P.; Meng, K.; Wang, S. F. Graphene Oxide Based Photoinduced Charge Transfer Label-Free Near-Infrared Fluorescent Biosensor for Dopamine. *Anal. Chem.* **2011**, *83*, 8787−8793.

(32) Cheng, R.; Liu, Y.; Ou, S.; Pan, Y.; Zhang, S.; Chen, H.; Dai, L.; Qu, J. Optical Turn-On Sensor Based on Graphene Oxide for Selective Detection of D-Glucosamine. *Anal. Chem.* **2012**, *84*, 5641−5644.

(33) Kundu, A.; Layek, R. K.; Nandi, A. K. Enhanced Fluorescent Intensity of Graphene Oxide−Methyl Cellulose Hybrid in Acidic Medium: Sensing of Nitro-Aromatics. *J. Mater. Chem.* **2012**, *22*, 8139−8144.

(34) Kundu, A.; Layek, R. K.; Kuila, A.; Nandi, A. K. Highly Fluorescent Graphene Oxide-Poly(vinyl alcohol) Hybrid: An Effective Material for Specific Au^{3+} Ion Sensors. *ACS Appl. Mater. Interfaces* **2012**, *4*, 5576−5582.

(35) Kundu, A.; Nandi, S.; Layek, R. K.; Nandi, A. K. Fluorescence Resonance Energy Transfer from Sulfonated Graphene to Riboflavin: A Simple Way to Detect Vitamin B_2. *ACS Appl. Mater. Interfaces* **2013**, *5*, 7392−7399.

DOI: 10.1021/am507110r
ACS Appl. Mater. Interfaces 2015, 7, 3512−3523

(36) Fang, M.; Wang, K.; Lu, H.; Yang, Y.; Nutt, S. Covalent Polymer Functionalization of Graphene Nanosheets and Mechanical Properties of Composites. *J. Mater. Chem.* **2009**, *19*, 7098−7105.
(37) Shen, J.; Hu, Y.; Li, C.; Qin, C.; Ye, M. Synthesis of Amphiphilic Graphene Nanoplatelets. *Small* **2009**, *5*, 82−85.
(38) Veca, L. M.; Lu, F.; Meziani, M. J.; Cao, L.; Zhang, P.; Qi, G.; Qu, L.; Shrestha, M.; Sun, Y. P. Polymer Functionalization and Solubilization of Carbon Nanosheets. *Chem. Commun.* **2009**, 2565−2567.
(39) Lee, S. H.; Dreyer, D. R.; An, J.; Velamakanni, A.; Piner, R. D.; Park, S.; Zhu, Y.; Kim, S. O.; Bielawski, C. W.; Ruoff, R. S. Polymer Brushes via Controlled, Surface-Initiated Atom Transfer Radical Polymerization (ATRP) from Graphene Oxide. *Macromol. Rapid Commun.* **2010**, *31*, 281−288.
(40) Kim, H.; Abdala, A. A.; Macosko, C. W. Graphene/Polymer Nanocomposites. *Macromolecules* **2010**, *43*, 6515−6530.
(41) He, H.; Gao, C. Supraparamagnetic, Conductive, and Processable Multifunctional Graphene Nanosheets Coated with High-Density Fe_3O_4 Nanoparticles. *ACS Appl. Mater. Interfaces* **2010**, *2*, 3201−3210.
(42) Kou, L.; He, H.; Gao, C. Click Chemistry Approach to Functionalize Two-Dimensional Macromolecules of Graphene Oxide Nanosheets. *Nano-Micro Lett.* **2010**, *2*, 177−183.
(43) Xu, Z.; Gao, C. *In situ* Polymerization Approach to Graphene-Reinforced Nylon-6 Composites. *Macromolecules* **2010**, *43*, 6716−6723.
(44) Kan, L.; Xu, Z.; Gao, C. General Avenue to Individually Dispersed Graphene Oxide-Based Two-Dimensional Molecular Brushes by Free Radical Polymerization. *Macromolecules* **2011**, *44*, 444−452.
(45) Jiang, K.; Ye, C.; Zhang, P.; Wang, X.; Zhao, Y. One-Pot Controlled Synthesis of Homopolymers and Diblock Copolymers Grafted Graphene Oxide Using Couplable RAFT Agents. *Macromolecules* **2012**, *45*, 1346−1355.
(46) Deng, Y.; Zhang, J. Z.; Li, Y.; Hu, J.; Yang, D.; Huang, X. Thermoresponsive Graphene Oxide-PNIPAM Nanocomposites with Controllable Grafting Polymer Chains Via Moderate In Situ SET-LRP. *J. Polym. Sci., Part A: Polym. Chem.* **2012**, *50*, 4451−4458.
(47) Pan, Y.; Bao, H.; Sahoo, N. G.; Wu, T.; Li, L. Water-Soluble Poly(*N*-isopropylacrylamide)−Graphene Sheets Synthesized via Click Chemistry for Drug Delivery. *Adv. Funct. Mater.* **2011**, *21*, 2754−2763.
(48) Qi, J.; Lv, W.; Zhang, G.; Zhang, F.; Fan, X. Poly(*N*-isopropylacrylamide) on Two-Dimensional Graphene Oxide Surfaces. *Polym. Chem.* **2012**, *3*, 621−624.
(49) Mortisen, D.; Peroglio, M.; Alini, M.; Eglin, D. Tailoring Thermoreversible Hyaluronan Hydrogels by "Click" Chemistry and RAFT Polymerization for Cell and Drug Therapy. *Biomacromolecules* **2010**, *11*, 1261−1272.
(50) Bao, H.; Li, L.; Gan, L. H.; Ping, Y.; Li, J.; Ravi, P. Thermo and pH-Responsive Association Behavior of Dual Hydrophilic Graft Chitosan Terpolymer Synthesized via ATRP and Click Chemistry. *Macromolecules* **2010**, *43*, 5679−5687.
(51) Chen, J.; Liu, H.; Zhao, C.; Qin, G.; Xi, G.; Li, T.; Wang, X.; Chen, T. One-step Reduction and PEGylation of Graphene Oxide for Photothermally Controlled Drug Delivery. *Biomaterials* **2014**, *35*, 4986−4995.
(52) Zhao, X.; Liu, P. Biocompatible Graphene Oxide as a Folate Receptor Targeting Drug Delivery System for the Controlled Release of Anti-cancer Drugs. *RSC Adv.* **2014**, *4*, 24232−24239.
(53) Song, E.; Han, W.; Li, C.; Cheng, D.; Li, L.; Liu, L.; Zhu, G.; Song, Y.; Tan, W. Hyaluronic Acid-Decorated Graphene Oxide Nanohybrids as Nanocarriers for Targeted and pH-Responsive Anticancer Drug Delivery. *ACS Appl. Mater. Interfaces* **2014**, *6*, 11882−11890.
(54) Zhao, X.; Liu, L.; Li, X.; Zeng, J.; Jia, X.; Liu, P. Biocompatible Graphene Oxide Nanoparticle-Based Drug Delivery Platform for Tumor Microenvironment-Responsive Triggered Release of Doxorubicin. *Langmuir* **2014**, *30*, 10419−10429.
(55) Xu, Z.; Wang, S.; Li, Y.; Wang, M.; Shi, P.; Huang, X. Covalent Functionalization of Graphene Oxide with Biocompatible Poly(ethylene glycol) for Delivery of Paclitaxel. *ACS Appl. Mater. Interfaces* **2014**, *6*, 17268−17276.
(56) Tonnesen, H. H.; Karlsen, J. Alginate in Drug Delivery Systems. *Drug Dev. Ind. Pharm.* **2002**, *28*, 621−630.
(57) Marcano, D. C.; Kosynkin, D. V.; Berlin, J. M.; Sinitskii, A.; Sun, Z.; Slesarev, A.; Alemany, L. B.; Lu, W.; Tour, J. M. Improved Synthesis of Graphene Oxide. *ACS Nano* **2010**, *4*, 4806−4814.
(58) Ferrari, A. C.; Meyer, J. C.; Scardaci, V.; Casiraghi, C.; Lazzeri, M.; Mauri, F.; Piscanec, S.; Jiang, D.; Novoselov, K. S.; Roth, S.; Geim, A. K. Raman Spectrum of Graphene and Graphene Layers. *Phys. Rev. Lett.* **2006**, *97*, 187401.
(59) Knight, D. S.; White, W. B. Characterization of Diamond Films by Raman Spectroscopy. *J. Mater. Res.* **1989**, *4*, 385−393.
(60) Jung, I.; Dikin, D.; Park, S.; Cai, W.; Mielke, S. L.; Ruoff, R. S. Effect of Water Vapor on Electrical Properties of Individual Reduced Graphene Oxide Sheets. *J. Phys. Chem. C* **2008**, *112*, 20264−20268.
(61) DeMichelis, F.; Schreiter, S.; Tagliaferro, A. Photoluminescence in a C:H Films. *Phys. Rev. B* **1995**, *51*, 2143−2147.
(62) Eda, G.; Lin, Y. Y.; Mattevi, C.; Yamaguchi, H.; Chen, H. A.; Chen, I. S.; Chen, C. W.; Chhowalla, M. Blue Photoluminescence from Chemically Derived Graphene Oxide. *Adv. Mater.* **2010**, *22*, 505−509.
(63) Pan, D.; Zhang, J.; Li, Z.; Wu, M. Hydrothermal Route for Cutting Graphene Sheets into Blue-Luminescent Graphene Quantum Dots. *Adv. Mater.* **2010**, *22*, 734−738.
(64) Wan, X. G.; Dong, J. M.; Xing, D. Y. Optical Properties of Carbon Nanotubes. *Phys. Rev. B* **1998**, *58*, 6756−6759.
(65) Zhao, W.; Song, C.; Pehrsson, P. E. Water-Soluble and Optically pH-Sensitive Single-Walled Carbon Nanotubes from Surface Modification. *J. Am. Chem. Soc.* **2002**, *124*, 12418−12419.
(66) Wang, C.; Cheng, L.; Liu, Z. Drug Delivery with Upconversion Nanoparticles for Multi-Functional Targeted Cancer Cell Imaging and Therapy. *Biomaterials* **2011**, *32*, 1110−1120.
(67) Kurapati, R.; Raichur, A. M. Graphene Oxide Based Multilayer Capsules with Unique Permeability Properties: Facile Encapsulation of Multiple Drugs. *Chem. Commun.* **2012**, *48*, 6013−6015.
(68) Flower, R. J. Drugs Which Inhibit Prostaglandin Biosynthesis. *Pharm. Rev.* **1974**, *26*, 33−67.
(69) Jain, A. K. Solubilization of Indomethacin using Hydrotropes for Aqueous Injection. *Eur. J. Pharm. Biopharm.* **2008**, *68*, 701−714.
(70) Tayyab, S.; Haq, S. K.; Aziz, M. A.; Khan, M. M.; Muzammil, S. Effect of Lysine Modification on the Conformation and Indomethacin Binding Properties of Human Serum Albumin. *Int. J. Biol. Macromol.* **1999**, *26*, 173−180.

DOI: 10.1021/am507110r
ACS Appl. Mater. Interfaces 2015, 7, 3512−3523